Advances in Polymer Technology

3D simulation and parametric analysis of polymer melt flowing through spiral mandrel die for pipe extrusion

Journal:	*Advances in Polymer Technology*
Manuscript ID	ADV-01-18-013.R2
Wiley - Manuscript type:	Research Article
Date Submitted by the Author:	30-Nov-2018
Complete List of Authors:	Nie, Yi; University of Nottingham - Ningbo China, Department of Mechanical, Materials and Manufacturing Engineering Hao, Jing; University of Nottingham - Ningbo China, Department of Mechanical, Materials and Manufacturing Engineering Lin, Yueh-Jaw ; University of Nottingham - Ningbo China, Department of Mechanical, Materials and Manufacturing Engineering Sun, Wei; University of Nottingham, UK, Department of Mechanical, Materials and Manufacturing Engineering
Keywords:	extrusion, spiral mandrel die, 3D simulation, polymer melt

3D simulation and parametric analysis of polymer melt flowing through spiral mandrel die for pipe extrusion

Yi Nie[1], Jing Hao[1], Yueh-Jaw Lin[1], Wei Sun[2]

[1]Department of Mechanical, Materials and Manufacturing Engineering, University of Nottingham Ningbo China

[2]Department of Mechanical, Materials and Manufacturing Engineering, University of Nottingham, UK

Correspondence to: Yi Nie; email: Yi.NIE@nottingham.edu.cn.

Abstract

With the increasing demands for large scale and high productivity, polymer pipes are recently produced using the advanced spiral mandrel dies. However, the fundamental research related to polymer melt flow mechanism in the spiral mandrel die for pipe extrusion is lagging behind. In the present study, the mathematical model for such a complex three-dimensional non-isothermal viscous flow of polymer melts obeying power law model was developed based on computational fluid dynamics (CFD) theory. Finite volume element method was applied to predict the rheological behaviours of polymer melt flowing through the complex flow channel. The essential flow characteristics including velocity, pressure drop, wall shear stress and temperature were investigated. The effects of both mandrel structure parameters and mass flow rate upon the flow patterns were further discussed. Some recommendations on spiral mandrel die design for pipe production were put forward.

Keywords: Extrusion, Spiral mandrel die, 3D simulation, Polymer melt.

1 Introduction

With the increasing demand towards large diameter and high productivity, plastic pipes are recently produced using the advanced spiral mandrel dies instead of the traditional spider die heads. A typical spiral mandrel die, shown as Fig. 1, consists of an outer die body and an inner mandrel with helical grooves cut in the mandrel surface. The polymer melts enter the spiral grooves and flow around the perimeter of the mandrel. An amount of melts will leak in the axial direction towards the next spiral groove. As the depth of the spiral grooves reduce with distance, the spiral flow decreases and the leakage flow increases gradually. When the depth of spiral groove reaches zero, the flow is completely transferred to annular axial flow [1, 2]. The main advantage of the spiral mandrel die lies in the way it distributes the polymer melts. The gradual leakage of the polymer melts out of the spiral grooves as it traverses around the circumference results in a layering effect. This layering effect provides some additional mixing or homogenization of the polymer melts giving more uniformity to the product. Besides, the absence of mandrel support elements can avoid the appearance of weld lines on the extruded polymer pipe [3].

Since the geometry of spiral mandrel die is quite complex, it is important to investigate the related polymer forming mechanism for a good die design. Earlier research on flow pattern in spiral mandrel dies mainly used the control volume method, in which the annular flow field was spread out and discretised into many control volumes [4-9]. The earliest analysis using control volume method was presented by Proctor [4]. A detailed review and evaluation of the control volume method based models was published by C-C Huang [9]. But it is known that the control volume method based models involved separate one-dimensional or two-dimensional simulation which can only roughly calculate

the circumferential distribution of spiral flow and leak flow. The advances in computing power have made 3D simulation a viable and practical tool for an improved understanding of the complex flow phenomena in spiral mandrel dies.

The first 3D simulation of a spiral mandrel die is believed to be performed by Coyle and Perdikoulias [10] in 1991. Skabrahova et al. [11] analysed the effect of variation of flow rate at the inlet of the different spirals on the velocity and temperature distributions at the exit of the die. Perdikoulias et al. [12] suggested a method of analysing and comparing the performance of spiral mandrel dies based upon the simulation performed using the Compuplast®, Virtual Extrusion Laboratory™ 3D FEM module. Sun and Gupta [13] performed a three-dimensional non-isothermal simulation of the flow in a spiral mandrel die using the PELDOM software and studied the effect of the elongational viscosity of a low-density polyethylene on the flow in the die. Apart from the cylindrical spiral mandrel dies, Zatloukal et al. [14] studied the flow of a polymer melt through a flat spiral distribution system used in "stacked" type dies through three-dimensional finite element simulations. Yilmaz et al. [15] analysed the flow filed characteristics through a conical spiral mandrel die by 3D Computational Fluid Dynamics simulation. The previous researches have shown that numerical simulation as a highly effective method can well predict material forming mechanisms in spiral mandrel dies. However, it is found that most of recent researches about spiral mandrel dies mainly aim at blown film production with limited attention on plastic pipe extrusion, which shows different flow characteristics. Besides, most of the recent researches are found aiming at solving supposed or simplified numerical examples, including the hypothesis of material parameters and flow

domain geometries. From an industrial viewpoint, more rigorous strategies to solve practical flow problems in the spiral mandrel plastic pipe die are needed.

With the advance of numerical computing techniques, the three-dimensional rheological behaviour of HDPE flowing through the flow channel of spiral mandrel die for pipe extrusion is investigated in the paper. The mathematical model of 3D non-isothermal viscous flow of polymer melt obeying a Power Law model is established based on the computational fluid dynamics (CFD) theory. The geometric and numerical model are built up according to practical engineer drawings and processing parameters. The SIMPLEC algorithm based on finite volume method is implemented for the prediction of the non-isothermal viscous flow patterns. The distributions of essential flow characteristics including flow velocity, pressure drop, wall shear stress and melt temperature, are investigated. The effects of both mandrel structure and processing parameters upon the flow patterns are further investigated. Some recommendations on practical manufacturing control of such extrusion process are thus concluded.

2 Extrusion process of plastic pipe using spiral mandrel die

Fig. 2(a) shows a typical pipe extrusion line (model FLSJ150-36DG) from Ningbo Graewe-Fangli Extrusion equipment Co., LTD. During the extrusion process, the resin hopper is used to convey the raw materials to the extruder at a certain feeding speed. Polymer pellets mixed in a certain proportion are then heated and extruded by the single-screw extruder. The extrusion die is an assembly with a flow channel to form the fused polymer melts into the final or near-final shape prior to sizing. To produce a large scale HDPE pipe with the maximum diameter of 1200 mm, the spiral mandrel die

shown in Fig. 2(b) is applied to evenly distribute and mix the polymer melts. After shaped and cooled in the following vacuum sizing tank, the plastic pipe can be obtained.

Compared with blown film production, the spiral mandrel die for pipe production has the structure as sketched in Fig. 3. The distribution section is to divide polymer melts into several streams to supply the following 24 spiral channels. Both the spiral flow and corresponding leakage flow will take place in the following spiral section. It is expected that homogeneous thermal and physical distribution of polymer melts along the circumference is obtained at the exit of the spiral section. To produce the large scare plastic pipe, an expansion section is designed with the diameter of flow channel increasing gradually. The adapter section is designed to develop a steady annular flow of polymer melts, which is ready to be shaped to the required size. After contraction and parallel, the preliminarily shaped polymer melts will flow out of the extrusion die. The flow channel shows that the polymer melts experience complex shear and deformation in several flow sections during the extrusion process. This leads to some special flow properties of polymer melts which will be investigated by means of 3D numerical simulation in the following contents.

3 Modelling of the extrusion process

3.1 governing equations

The governing equations to solve the three-dimensional polymer melt flow problem in spiral mandrel die for pipe production includes continuity, momentum and energy equations according to the computational fluid dynamics (CFD) theory [16]. Considering the incompressible steady laminar

flow characteristics of polymer melts in the flow channel when a successive extrusion process is arrived, the governing equations are simplified as follows

$$\nabla \cdot \vec{v} = 0 \tag{1}$$

$$\nabla \cdot \boldsymbol{\tau} - \nabla p = 0 \tag{2}$$

$$\rho c_v \vec{v} \cdot \nabla T = -\nabla \cdot \vec{q} + Q \tag{3}$$

where ∇ is the Hamilton differential operator, $\vec{v}$ is the velocity vector, $\boldsymbol{\tau}$ is the deviatoric stress tensor, p is the hydrostatic pressure, ρ is the material density, c_v is the heat capacity, T is the temperature, $\vec{q}$ is the heat flux and Q is the total source term.

The heat flux Fourier's law of heat conduction is assumed to have an isotropic thermal conductivity $\vec{q} = -k\nabla T$ for this steady flow. Therefore, the energy equation, Equation (3), can be rewritten as

$$\rho c_v \vec{v} \cdot \nabla T = k\nabla^2 T + Q \tag{4}$$

where k is the isotropic thermal conductivity based on the heat flux Fourier's Law.

The polymer melt in the flow channel is regarded as a viscous flow and all the mechanical energy is assumed to be dissipated as heat and the total source term Q is assumed to be equal to viscous heat dissipation [17] as follows

$$Q = \boldsymbol{\tau}:\boldsymbol{\varepsilon} \tag{5}$$

where $\boldsymbol{\varepsilon} = (\nabla\vec{v} + (\nabla\vec{v})^T)/2$ is the strain rate tensor.

The following constitutive equation is adopted to describe the relationship of stress and strain for the viscous fluid flow

$$\boldsymbol{\tau} = 2\eta\boldsymbol{\varepsilon} \tag{6}$$

where η is the apparent viscosity, which is described by the Power Law equation in this paper [18]

$$\eta = K\dot{\gamma}^{n-1} \tag{7}$$

where $\dot{\gamma} = \sqrt{2\boldsymbol{\varepsilon}:\boldsymbol{\varepsilon}}$ is the shear rate (invariant of the strain rate tensor), K is the consistency factor and n is the power-law (or non-Newtonian) index with a value between 0 and 1. The coupling between the momentum and energy equation is simplified by not considering the temperature dependence of material property, which means that calculated temperature by energy equation is assumed to have no effect on the viscosity of the polymer melts.

3.2 Geometric model and boundary conditions

According to the above-proposed three-dimensional non-isothermal viscous flow model, flow characteristics of polymer melts in the spiral mandrel die for pipe production is investigated as sketched in Fig. 4. Four different views of the flow channel is respectively shown in Fig. 4(a)-(d). Its geometric parameters are listed in Table 1. A kind of important engineering material HDPE is adopted for the large scale pipe production. Its essential rheological parameters are listed in Table 2 [19].

As the flow channel in the spiral mandrel die is cyclic symmetry for each 60°, a 1/6 of the flow channel model was considered to reduce the computational calculation time, as shown in Fig. 5. Tetrahedral elements were used to mesh the distribution, spiral and relaxation sections, while hexahedral elements were used to mesh the following sections. 3 lays of inflation elements were applied for the leakage channel in the spiral section. The meshes on the symmetrical surfaces matches each other. The geometric model of the flow channel is divided into 1138374 elements and 307420 nodes.

Boundary conditions are required at the boundary faces of the computational domain during the numerical simulation. A fully developed fluid flow is imposed on the inlet boundary. For the polymer

material with power law constitutive model, the fully developed velocity component with mass flow rate Q_m at inlet is as follows [3]:

$$v_x = 0 \tag{8}$$

$$v_y = \frac{Q_m(m+3)}{\rho\pi R^{m+3}}\left(\frac{R^{m+1} - \left(x^2+z^2\right)^{\frac{m+1}{2}}}{m+1}\right) \tag{9}$$

$$v_z = 0 \tag{10}$$

where x, y and z are the global coordinate components of each node on the inlet cross-section. R is the radius of the cross section at inlet. m is the flow exponent and equal to $1/n$. A fixed temperature $T = 210℃$ is imposed on the inlet boundary according to the actual working condition. On the outlet cross-section, values of the relative pressure and the streamwise gradient for temperature are set to be zero. As shown in Fig. 5, the finite element model of the flow channel contains both inner and outer walls. Non-slip boundary condition is applied at the walls, which indicates that the velocity components of polymer melts contacted to the walls are $v_x = v_y = v_z = 0$. An insulated condition is also imposed to the walls and the temperature rise of polymer melt in the flow channel is due to viscous heat dissipation with ignoring outer thermal conductivity. The periodic surfaces, as shown in Fig. 5, are specified as a pair of periodic boundary condition where both the pressure drop and heat transfer are 0.

3.3 Numerical algorithm

An element-based finite volume method is used in this study [20], which first involves discretizing the spatial domain using a mesh. The mesh is used to construct finite volumes, which are used to conserve relevant quantities such as mass, momentum and energy. Thus, the governing equations

described in section 3.1 can be integrated over each cell. The governing equation for each cell is described as

$$\sum_{f}^{N_{faces}} \rho \overrightarrow{V_f} \cdot \overrightarrow{A_f} = 0 \tag{11}$$

$$\sum_{f}^{N_{faces}} \boldsymbol{\sigma_f} \cdot \overrightarrow{A_f} - \sum_{f}^{N_{faces}} p_f \vec{I} \cdot \overrightarrow{A_f} = 0 \tag{12}$$

$$\sum_{f}^{N_{faces}} \rho c_v \overrightarrow{v_f} T_f \cdot \overrightarrow{A_f} = \sum_{f}^{N_{faces}} k \nabla T_f \cdot \overrightarrow{A_f} + QV \tag{13}$$

where N_{faces} donates the number of faces enclosing cell, $\overrightarrow{A_f}$ is surface area vector of element face f, $\overrightarrow{v_f}$ is the velocity through element face f, p_f is the hydrostatic pressure at face f, T_f is the temperature at face f, $\boldsymbol{\sigma_f}$ is the stress tensor at face f and $\vec{I}$ is the identity matrix.

Equation (11) will be linearized for a pressure correction according to the SIMPLEC algorithm in this paper [21]. Similar equations can be written for each cell in the mesh. This results in a set of algebraic equations with a sparse coefficient matrix. For scalar equations, this linear system can be solved using a point implicit (Gauss-Seidel) linear equation solver in conjunction with an algebraic multigrid (AMG) method.

It is know that the face values ϕ_f (including V_{fx}, V_{fy}, V_{fz}, p_f, T_f) are required for the convection terms in the governing equations (11-13) and must be interpolated from the cell centre values ϕ. The second-order upwind scheme is applied to compute the face values ϕ_f as shown in literature [22]. Besides, the gradient term $\nabla\phi$ is also required to discretize the convection and diffusion terms in the flow conservation equations. The Least Square Cell-Based method is selected to compute the gradient term $\nabla\phi$ as shown in literature [23].

4 Results and discussion

A mass flow rate of 1100 kg/h with a preheating temperature of 210 ℃ was assigned at the inlet according to the actual working condition. The commercial software FLUENT is used to solve the above numerical problem. The calculation is converged after 60 steps. The essential flow characteristics of polymer melts in the spiral mandrel die for pipe extrusion are investigated by assessments of principal field variables including flow velocity, pressure drop, wall shear stress and melt temperature.

4.1 Essential flow characteristics

4.1.1 Streamline analysis

The streamline of polymer melts in the flow channel is shown in Fig. 6. It demonstrates that the polymer melt flow is firstly developed into annular flow by the cone near the die entrance. The annular flow is then gradually divided into 24 streams by the coathanger distributor before they reach at the 24 ports of spiral channels. Each melt stream will then flow correspondingly to their own spiral grooves. The melt flowing through one spiral groove divides itself into two streams as the depth of spiral channel decreases. The first stream flows over a land formed between two spiral grooves and becomes leakage flow. The other continues to flow through the spiral course. It is found that as the depth of the spiral channel reduces along the axial direction, the spiral flow decreases, and at the same time the leakage flow increases gradually. A newly developed axial flow is found at the exit of spiral section. It is then released by shear stress with the expansion of cross-section in relaxation section. In the following expansion and adapter sections, the expansion flow and a steady annular flow is

developed, correspondingly. The steady melt flow is converted to the required shape and dimension through the later contraction and parallel sections.

It is found that the method in most previous researches to only divide the flow in spiral section into spiral flow and axial leakage flow is inaccurate. Fig. 7 shows the velocity distribution at the cross-section vertical to axial direction in spiral section. As shown in Fig. 7, the melts flow could be divided into 4 parts (refer to number of pots) along the spiral direction for each periodic unit. Each part consists of 3 elements which are element A of spiral flow in spiral groove, element B of leakage flow under spiral groove and element C of leakage flow between spiral grooves. As shown in Fig. 6, the melt in element B and C do not always flow along axis. The flow in element B mainly comes from element A in previous cross-section due to the gradually reduction of depth of spiral groove. It will still flow along the spiral direction due to the drag by polymer melts in element A. The polymer in element C comes from previous element B due to the helix of spiral groove. The polymer melts in element C has a respectively bigger axial flow speed compared with element B which is mainly driven by the axial pressure drop and surround flow in element B. As the melts flow transfers from element A to B and to C, the flow will gradually become to axial flow at the exit of spiral zone. The results show that it is important to suitably design the dimension of element A, B and C so as to make the melts reaches uniform steadily and quickly.

4.1.2 Velocity analysis

Fig. 8 shows the distribution tendency of flow velocity on the periodic plane. It can be found that the velocity is the maximum near the entrance of the flow channel because of the smallest cross-section area in this region as shown in Fig. 8(b). Fig. 8(c) and (d) show the axial and circumferential

components of flow velocity at the periodic plane in the spiral section, respectively. It is the evident that the axial velocity increases and circumferential velocity decreases as the spiral groove winds around the mandrel. The reduction in circumferential velocity is important because a good mandrel design requires the circumferential velocity to vanish at the exit of spiral section.

In order to better quantify flow pattern, the velocity at the centreline of the annular cross-section in flow channel is studied as shown in Fig. 9. The velocity at the centreline of the annular exit of the spiral section is plotted in Fig. 10. It shows that there is slight fluctuation of velocity at the centreline which is due to the inertia of previous spiral flows. It is calculated that the flow velocity at the centreline has a relative standard deviation of 2.71%, which indicates that there exists a relative uniform flow distribution at spiral section outlet. Fig. 10 also shows the velocity distribution at the centreline at the exit of other sections. It demonstrates that the exit of relaxation zone (y=0.535 m) has a more uniform distribution of velocity at the centreline than that of exit of spiral zone. This means that relaxation zone has a function of making the melt flow reach a better circumferential distribution. It is also found that the flow already has a complete uniform distribution of velocity at the centreline at the exit of expansion section (y=0.945 m), which is far from the exit of the parallel. The results indicates that the design limitation of the following adapter, contraction and parallel zones can be greatly released compared with traditional extrusion die (e.g. spider extrusion die).

4.1.3 Pressure analysis

Pressure drop of polymer melts is an important parameter from which we can assess energy consumption during the extrusion process. Fig. 11 shows the pressure distribution along the axial direction. It can be found that the pressure has a great reduction from the die inlet to the exit of spiral

section (y=0.405 m). The flow in the relaxation and expansion sections have a gentle decrease of pressure, while there is relatively no pressure drop in the following adapter, contraction and parallel sections. The maximum pressure of 13.1 MPa exists at the die inlet. It also shows that there is a jump pressure drop near the exit of distribution zone. This is due to that the coathanger distribution channel is vertical to the axial direction. That is why it is suggested to design an inclination angle for the distribution channel to fit with the flow behaviour of polymer melts and avoid the jump pressure drop. The pressure distribution on the outer wall in the spiral section is shown in Fig. 12(a). It indicates that the pressure contour line is vertical to the spiral groove near the entrance of the spiral section and gradually becomes vertical to the axial direction when polymer melts flow out of the spiral section. Fig. 12(b) shows the pressure distribution at the cross-section (y=0.3 m) of the spiral section. The pressure distribution can be divided into 4 parts refer to periodic character. For each periodic element, the pressure gradually decreases along the circumference. The results also shows that it is not suitable to simply divide the flow in the spiral section into spiral flow and axial leakage flow.

4.1.4 Wall shear stress analysis

Distribution of flow stress is an important factor that affects polymer melt structure like orientation degree which can directly influence the physical performance of the final product. It is known that the polymer melts are subject to much stronger shear near the distribution and spiral sections, the wall shear stress distributions on these two sections are focused as shown in Fig. 13. It can be found that the maximum wall shear stress happens near the die inlet, and there is much shear stress found in the spiral section which can generate huge viscous heat in the polymer melts. The flow in the distribution and spiral sections should be well controlled as too high shear stress will result in the quality problems

like melt fracture. It is also found that the wall shear stress in the region past the spiral (element C shown in Fig. 7(b)) is higher than that in the spiral channels (elements A and B shown in Fig. 7(b)), which indicates that the shear stress is enough to generate the viscous flow of polymer melt among spirals. The results also show that there are nearly no wall shear stresses at some corners in the distribution section. The polymer melts which do not suffer enough shearing may lead to flow stagnation. So it is also suggested that the distribution channel is designed with an inclination angle to the axial direction. Besides, the initial thickness of leakage gap should be 0, theoretically. But it is designed to be 0.001 m in practical for the feasibility of assembly. That's why the wall shear stresses at the plots of spiral channels are nearly zero. Stagnation may also happen here.

4.1.5 Temperature analysis

It is known that high temperature may cause melts degradation or earlier crosslink of the polymer melts. Good prediction of thermal effect is of much importance. Fig. 14 shows the temperature along the axial direction. It can be found that the temperature keeps rising from the intake to the spiral section, and the temperature reaches the highest at the exit of spiral zone. As the polymer melts start to be redistributed and suffer a relatively weaker shear, there is a slightly temperature decrease in the flowing relaxation and expansion sections. The temperature remains nearly unchanged along the axial direction until the polymer melts flow out of the extrusion die.

4.2 Effect of mandrel structure

It is a key factor for successful pipe extrusion die design to achieve uniform flow distribution in the cross direction on the outlet for the reason that it can reduce products residual stresses and prevent the

occurrence of curl distortions. The balance of flow distribution on the outlet cross-section is evaluated by the velocity relative deviation δU which is defined as

$$\delta U = \sqrt{\frac{\sum_{i=1}^{n}\left(\frac{v_i - \overline{v}}{\overline{v}}\right)^2}{n}} \times 100\% \quad (14)$$

where v_i is the flow velocity at each node on the outlet cross-section, $\overline{v}$ is the mean flow velocity at the outlet cross-section. n is the total number of nodes on the outlet cross-section. Different from the velocity variation discussed in section 4.1.2, the velocity relative deviation δU discussed in this section will take all the nodes in the annular cross-section into account, which can demonstrate the velocity variation in both circumferential and radial directions.

It is known that the mandrel structural parameters including initial depth of spiral groove H, end radius of mandrel R_3 (determines the taper angle of mandrel) and helix angle α are important for the pipe extrusion process using the spiral mandrel die. Their effects on the flow pattern are respectively discussed as follows.

The variations of initial depth of spiral groove can change the flux in spiral grooves and hence influence the flow balance. Six mandrel structures with different initial depths of spiral groove H (H= 0.036m, H= 0.040m, H= 0.044m, H= 0.048m, H= 0.052m, H= 0.056m) are employed to predict the effects on the flow pattern. Fig. 15(a) shows the variations of velocity relative deviation on both spiral section outlet and flow channel outlet versus different initial depths of spiral grooves. It is found that the velocity relative deviation almost keep near 32.00% as the increase of initial depths of spiral groove, which means the initial depth of spiral groove has little influence on the velocity relative deviation on spiral section outlet. Besides, it is found that the velocity relative deviation on flow channel outlet can

return to be about 25.00% from that on spiral section outlet. It means that the melts flow can be well redistributed in the downstream flow sections. As shown in Fig. 15(b), the pressure drop will be decreased with the increase of the initial depth of spiral groove. It is also found that there is a slight decrease of about 1 K of maximum temperature as the initial depth of spiral groove increases from 0.036m to 0.056m, shown in Fig. 15(c). That is to say, the initial depth of spiral groove could be increased to reduce the pressure drop with little impact on the balance of flow distribution and maximum temperature.

The difference of flow resistance in leakage between mandrel and die body resulted from different taper angles can affect the flow balance. Since the taper angle is greatly determined by the end radius of mandrel, six mandrel structure with different end radiuses of mandrel R_3 (R_3= 0.376m, R_3= 0.378m, R_3= 0.380m, R_3= 0.382m, R_3= 0.384m, R_3= 0.386m) are employed to investigate the effects of taper angle upon the flow characteristics of polymer melts. Fig. 16(a) shows the comparisons of velocity relative deviation on the spiral section outlet with different end radius of mandrel. It can be found that the velocity relative deviation on the spiral section outlet decreases with the increase of end radius of mandrel. Fig. 16(b) shows the variations of pressure drop versus different end radiuses of mandrel. It is found that the pressure drop increases about 10 MPa with the end radius of mandrel increasing 0.010 m. Besides, both the maximum wall shear stress and maximum temperature are greatly increased with the increase of end radius of mandrel as shown in Fig. 16(c) and (d), respectively. So, the increase of end radius of mandrel can improve the flow balance, but meanwhile increase the load required and viscous heat.

The variations of helix angle can change the spiral flow journeys and thus affect the flow balance in the spiral section. Six mandrel structures with different helix angles (α= 12°, α= 14°, α= 16°, α= 18°, α= 20°, α= 22°) are investigated in the study. As shown in Fig. 17(a), the increase of helix angle can result in the slightly increase of velocity relative deviation on the spiral section outlet. The pressure drop is reduced by almost 1 MPa as shown in Fig. 17(b). The maximum wall shear stress is decreased by about 5×10^4 Pa as shown in Fig. 17(c). As the shear stress can be weakened due to the increase of helix angle, the generated maximum temperature has a slightly decrease within 1K as shown in Fig. 17(d). Thus, the increase of helix can reduce the pressure drop and maximum temperature, but also lead to the deterioration of flow balance.

4.3 Effect of processing parameter

The mass flow rate is an important processing parameter for the pipe extrusion process. The flow characteristics of polymer melts flowing through the spiral mandrel die for pipe extrusion under different mass flow rates, 50 kg/h, 200 kg/h, 400 kg/h, 600 kg/h, 800 kg/h, 1000 kg/h, 1200 kg/h, 1400 kg/h, are investigated.

The variations of velocity relative deviations on spiral section outlet with different mass flow rates are shown in Fig. 18(a). It is found that the velocity relative deviation almost remain unchanged, which means that the variation of mass flow rate has little influence on the balance of flow distribution. The variations of pressure drop versus different mass flow rates are shown in Fig. 18(b). The result shows that the pressure drop increases about 2 folds with the mass flow rate increasing about 8 times. It is known that great deformation of extrusion die occurs when pressure drop exceeds critical value and extrusion problems like leakage may happen. So, the increase of mass flow rate can improve the

productivity, but meanwhile increase the probability of occurrence of production accident. As the variation of the pressure drop, the maximum wall shear stress and maximum temperature also increase with the increase of mass flow rate as respectively shown in Fig. 18(c) and (d).

The extrusion line is equipped with a pressure sensor to monitor the static pressure at the die inlet timely so as to indicate the pressure drop of the spiral mandrel die. Fig. 19 shows the relationship between the measured pressure drop and mass flow rate, together with the simulation result. Both the experimental and simulation results show that the pressure drop of the spiral mandrel die has a polynomial relation with the mass flow rate, which indicates that the simulation model is effective to describe the variation pattern of the extrusion process. However, the simulated pressure drop is found about 30% smaller than the experimental pressure drop. This is mainly due to that the constitutive model of the polymer melt is simplified using a Power Law model in the simulation which does not take the elongational viscosity property of the polymer melts [13].

6 Conclusions

The complex behaviours of HDPE flowing through the spiral mandrel die for pipe extrusion was predicted using a 3D numerical simulation framework. The SIMPLEC algorithm based on finite volume method incorporating algebraic multigrid (AMG) method has been implemented for the prediction of non-isothermal viscous flow patterns of polymer melts in the spiral mandrel die. The influences of both mandrel structure and processing parameters upon the melts flow characteristics were investigated. The simulated results are helpful for the control of processing conditions and the die design, and the following conclusions were obtained.

1. The flow in the spiral section is not just the combination of spiral flow in spiral grooves and axial flow in leakage. The 3D simulation showed a more complex flow which consists of the spiral flow in spiral grooves, leakage flow under spiral grooves and leakage flow between spiral grooves. The three flow parts influences each other and becomes the axial flow at the exit of the spiral section.
2. The velocity fluctuation along circumference at the spiral section outlet is found small compared with that of conventional extrusion die (eg. spider die). The design requirement for the following expansion, adapter, contraction, parallel sections can be greatly reduced.
3. Pressure drop mainly happens in the distribution and spiral sections. An inclination angle smaller than 90° to the axial direction for the distribution channel is suggested to avoid the jump pressure drop. Great wall shear stress and temperature rising is found in the distribution and spiral sections. More consideration should be taken here during the extrusion die design.
4. The velocity relative deviation δU is defined to evaluate the effects of mandrel structure upon flow balance. The increase of initial depth of spiral groove has little influence on velocity relative deviation at the spiral section outlet but can result in the decrease of pressure drop. The increase of end radius of mandrel can improve the flow balance, but meanwhile increase the load requirement and viscous heat. The increase of helix can reduce the pressure drop and maximum temperature, but lead to the deterioration of flow balance.
5. Under the same die structure, the increase of mass flow rate has little influence on the flow balance at the spiral section outlet. It can improve the productivity whereas the pressure drop,

the maximum wall shear stress and maximum temperature increase meanwhile. An optimal mass flow rate is of importance for both a high productivity and good final product quality.

6. The main advantage of the spiral mandrel distributor lies in its ability to create layers of polymer melts. It is foreseeable to quantify the degree of layering effect by analysing the cross-sectional micromorphology of the produced pipes in future work. Besides, further experiment to measure the temperature distribution of polymer melt should be conducted to verify the simulation results by scaling down the industrial spiral mandrel die into lab scale.

ACKNOWLEDGMENTS

The authors are grateful to Ningbo Science and Technology Bureau China for their kind support of the work through the Innovation Team Fund (Project Id: 2011B81006), Ningbo International Collaboration Fund (Project Id: 2011D10003), Ningbo Natural Science Foundation (Project ID: No.2011A610152). The work is also supported by National Natural Science Foundation of China (Project ID: 51305216). The authors are also grateful for the technical support by the Graewe-Fangli Extrusion equipment Co., LTD. Ningbo China.

REFERENCES

[1] D. G. Baird, D. I. Collias, Polymer processing: principles and design, 2nd ed., John Wiley & Sons, Hoboken, NJ, **2014**.

[2] Z. Tadmor, C. G. Gogos, Principles of polymer processing, 2nd ed., John Wiley & Sons, Hoboken, NJ, **2013**.

[3] W. Michaeli, Extrusion dies for plastics and rubber: design and engineering computations, 3rd ed., Hanser Verlag, Germany, **2003**.

[4] B. Procter, SPE J. **1972**, 28, 34.

[5] P. Saillard, J. Agassant, Polym. Proc. Eng. **1984**, 2, 37.

[6] E. Fahy, P. Gilmour, Int. J. Numer. Meth. Eng. **1986**, 23, 1.

[7] J. Perdikoulias, J. Vlcek, J. Vlachopoulos, Adv. Polym. Tech. **1987**, 7, 333.

[8] R. Rakos, D. Sebastian, Adv. Polym. Tech. **1990**, 10, 297.

[9] C. C. Huang, Polym. Eng. Sci. **1998**, 38, 573.

[10] D. J. Coyle, J. Perdikoulias, SPE ANTEC **1991**, 2445.

[11] P. Skabrahova, J. Svabik, J. Perdikoulias, ANTEC Conf. Proc. **2003**, 1, 305.

[12] J. Perdikoulias, J. Vlcek, J. Svabik, PLACE Conf. Proc. **2005**, 1, 115.

[13] Y. Sun, M. Gupta, Adv. Polym. Tech. **2006**, 25, 90.

[14] M. Zatloukal, C. Tzoganakis, J. Perdikoulias, P. Sáha, Polym. Eng. Sci. **2001**, 41, 1683.

[15] O. Yilmaz, E. Kısasöz, F. S. Guner, C. Nart, K. Kirkkopru, Fiber. Polym. **2014**, 15, 84.

[16] J. F. Wendt, Computational fluid dynamics: an introduction, Springer Science & Business Media, Germany, **2008**.

[17] Y. Mu, G. Zhao, A. Chen, X. Wu, Int. J. Adv. Manuf. Tech. **2013**, 67, 629.

[18] O.S. Carneiro, J. Nobrega, Design of Extrusion Forming tools, Smithers-Rapra, UK, **2012**.

[19] A. Naranjo, Plastics testing and characterization: industrial applications, Hanser Publications, Naperville, IL, **2008**.

[20] H. K. Versteeg, W. Malalasekera, An introduction to computational fluid dynamics: the finite volume method, 2nd ed., Pearson, UK, **2007**.

[21] J. Van Doormaal, G. Raithby, Numer. Heat. Tr. **1984**, 7, 147.

[22] T. Barth, D. Jespersen, AIAA 27th Aerospace Sciences Meeting **1989**, AIAA-89-0366.

[23] W. K. Anderson, D. L. Bonhaus, Comput. Fluids **1994**, 23, 1.

Table 1. Essential geometric parameters of the flow channel.

Geometric parameters	Values (mm)
Length of the distribution section ($L1$)	120
Length of the spiral section ($L2$)	325
Length of the relaxation section ($L3$)	125
Length of the expansion section ($L4$)	410
Length of the adapter section ($L5$)	760
Length of the contraction section ($L6$)	340
Length of the parallel section ($L7$)	170
Outer radius of outlet cross-section (R_o)	645
Inner radius of outlet cross-section (R_i)	550
Number of spiral channels	24
Helix angle (α)	14.357°
Width of initial spiral groove (W)	20
Initial depth of spiral groove (H)	48
Outer radius of die housing (R_1)	389
Initial radius of mandrel (R_2)	388
End radius of mandrel (R_3)	382

Table 2. Material property parameters of HDPE

Parameters	Values
Density ρ (kg/m^3)	750
Heat capacity per unit mass c_v (J/kg·℃)	2000
Thermal conductivity k (W/m·℃)	0.7
Power law index n	0.41
Consistency K (Pa·s)	21694.27

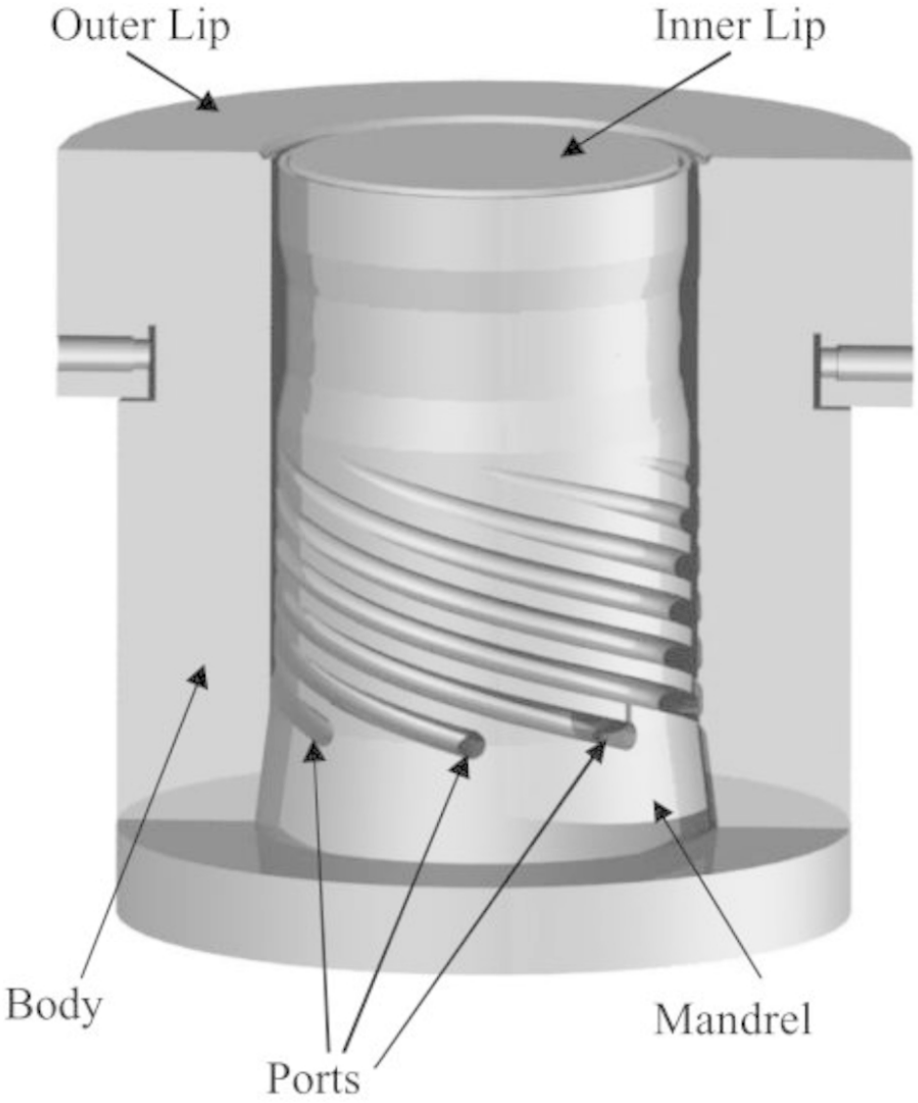

Fig. 1. A cut away view of a spiral mandrel die.

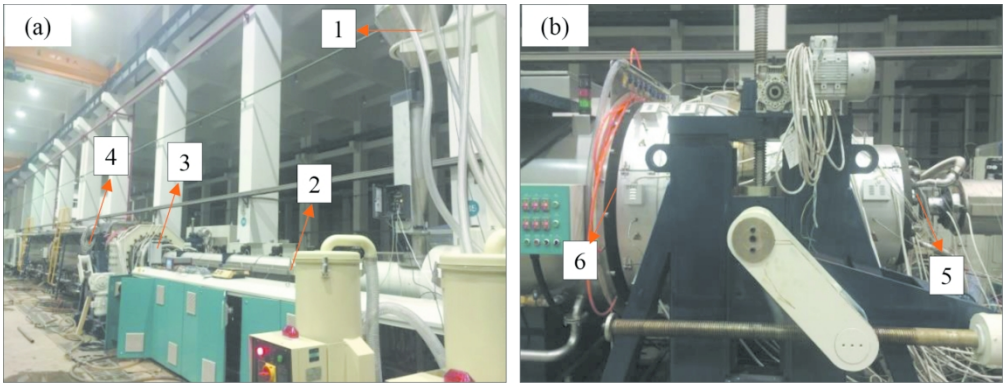

Fig. 2. The pipe extrusion line (Model FLSJ150-36DG) produced by Ningbo Graewe-Fangli Extrusion equipment Co., LTD (a: pipe extrusion line, b: spiral mandrel die. 1: resin hopper, 2: extruder, 3: extrusion die, 4: vacuum sizing tank, 5: die inlet, 6: die outlet).

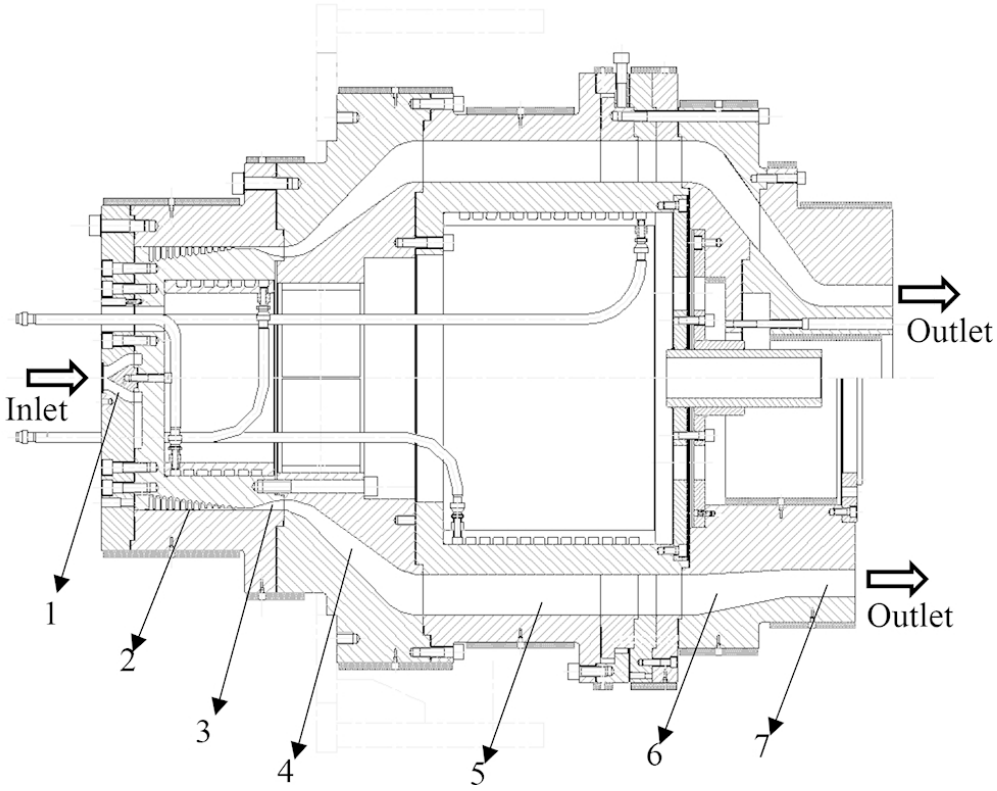

Fig. 3. Assembly diagram of the spiral mandrel die structure for production of a series of polymer pipes (1: distribution section, 2: spiral section, 3: relaxation section, 4: expansion section, 5: adapter section, 6: contraction section, 7: parallel section).

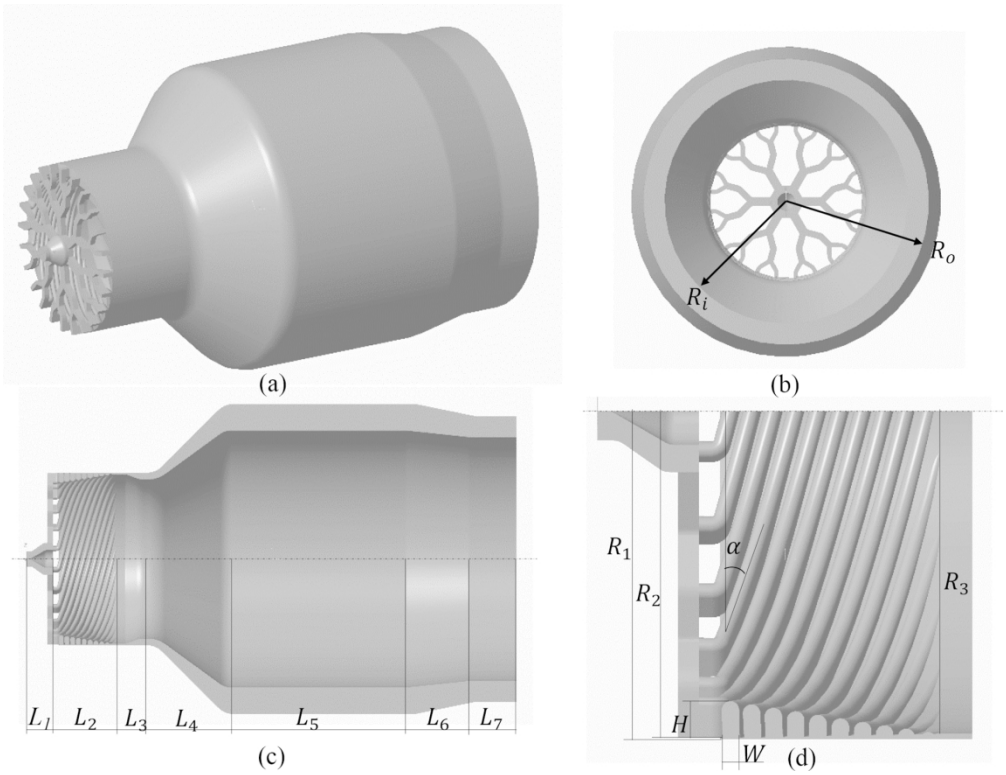

Fig. 4. Geometric model of the flow channel in the spiral mandrel die for pipe production (a: isometric view, b: right view, c: cross-sectional view, d: detailed view of spiral section).

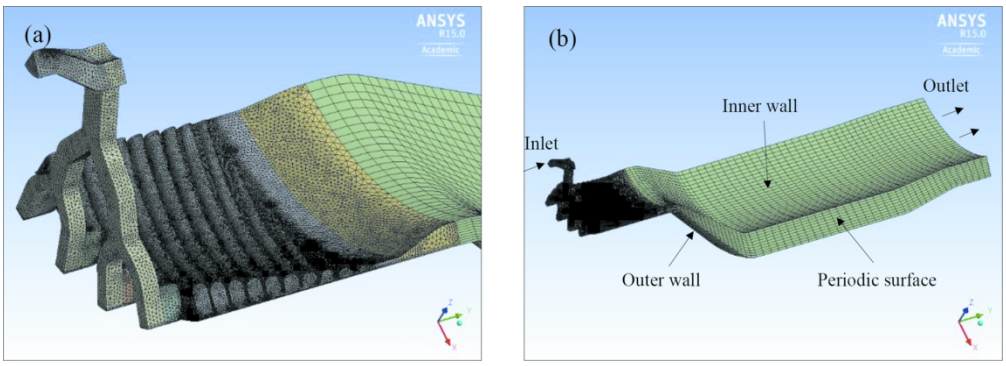

Fig. 5. Numerical model of the flow channel in spiral mandrel die for pipe extrusion (a: Tetrahedral mesh of distribution, spiral and relaxation sections, b: isometric view and the boundary surfaces).

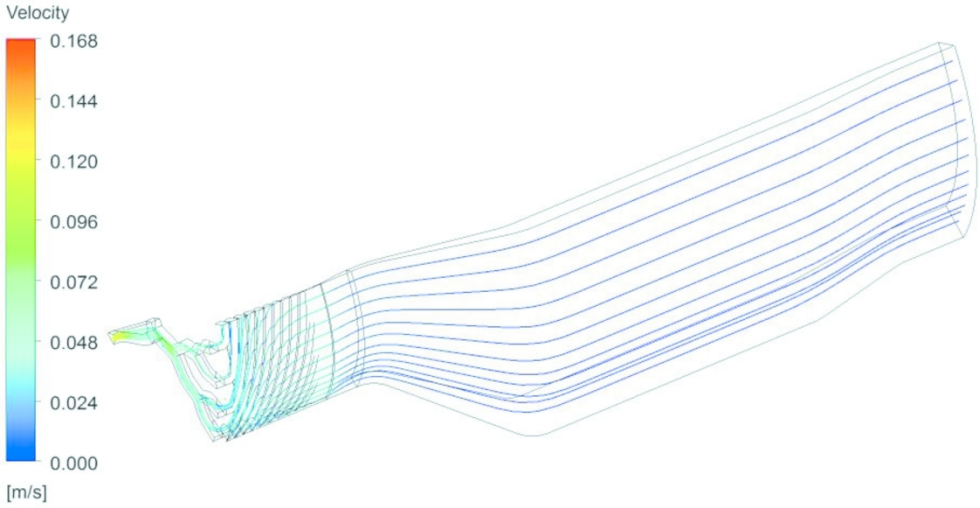

Fig. 6. Pathline of polymer melts flow in the spiral mandrel die.

169x86mm (300 x 300 DPI)

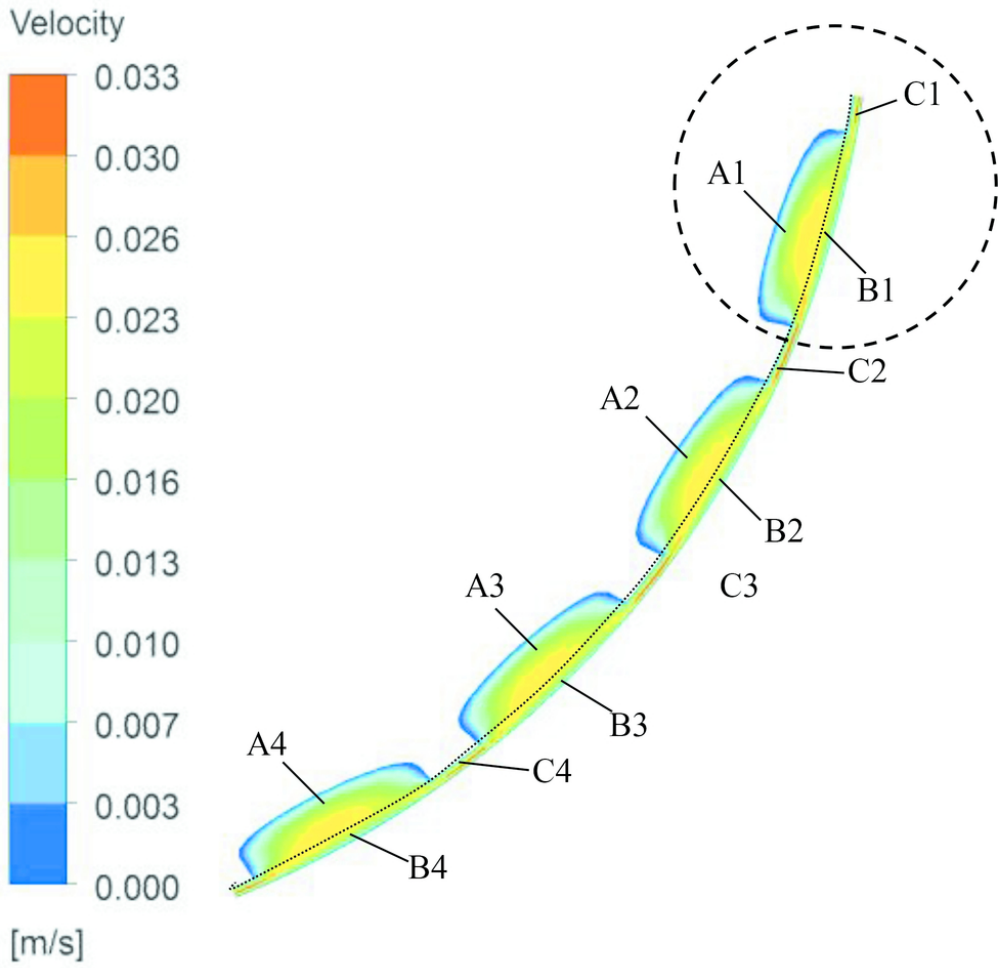

Fig. 7. Distribution of flow on the cross-section (y=0.3 m) vertical to axial direction in spiral section.

82x82mm (300 x 300 DPI)

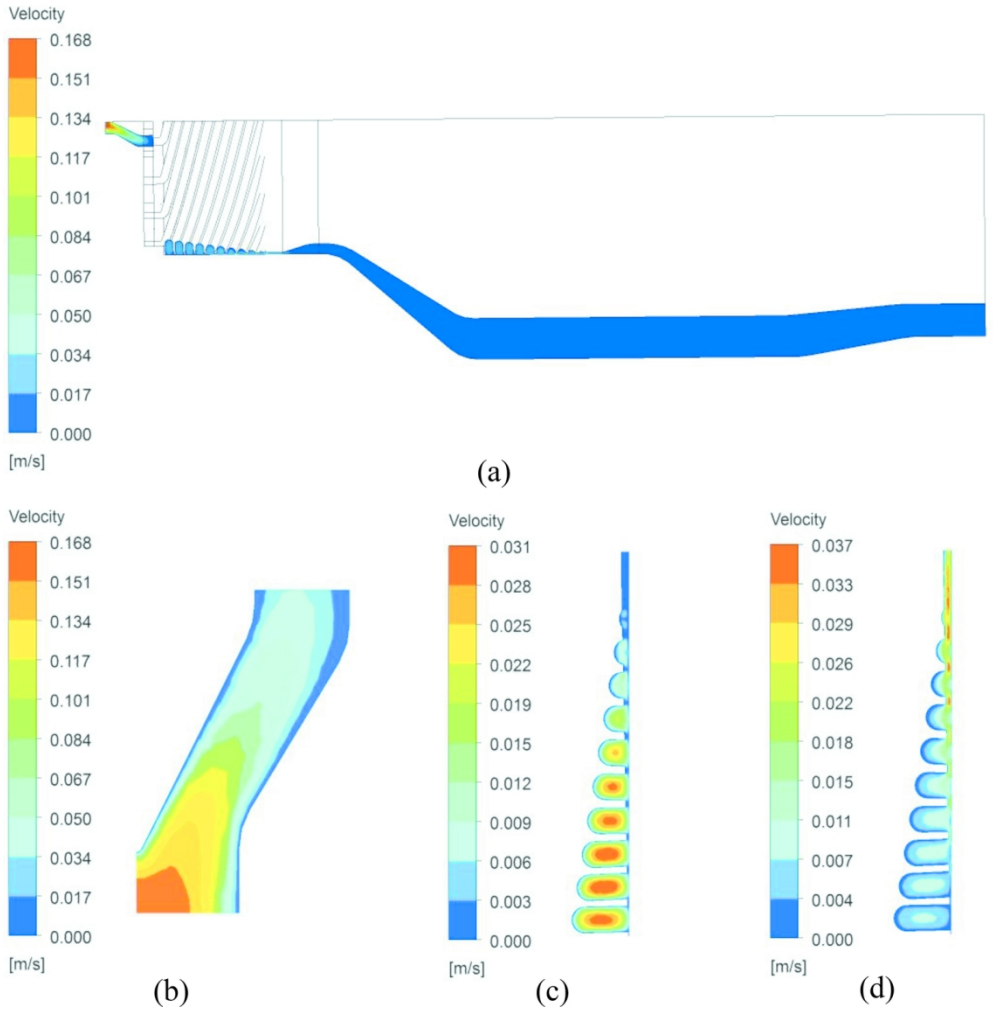

Fig. 8. Velocity distribution of the polymer melts flow (a: velocity contour on periodic surface in all sections; b: velocity contour on periodic surface near the flow entrance, c: contour of axial velocity on periodic surface in spiral section, d: contour of circumferential velocity on periodic surface in spiral section).

136x137mm (300 x 300 DPI)

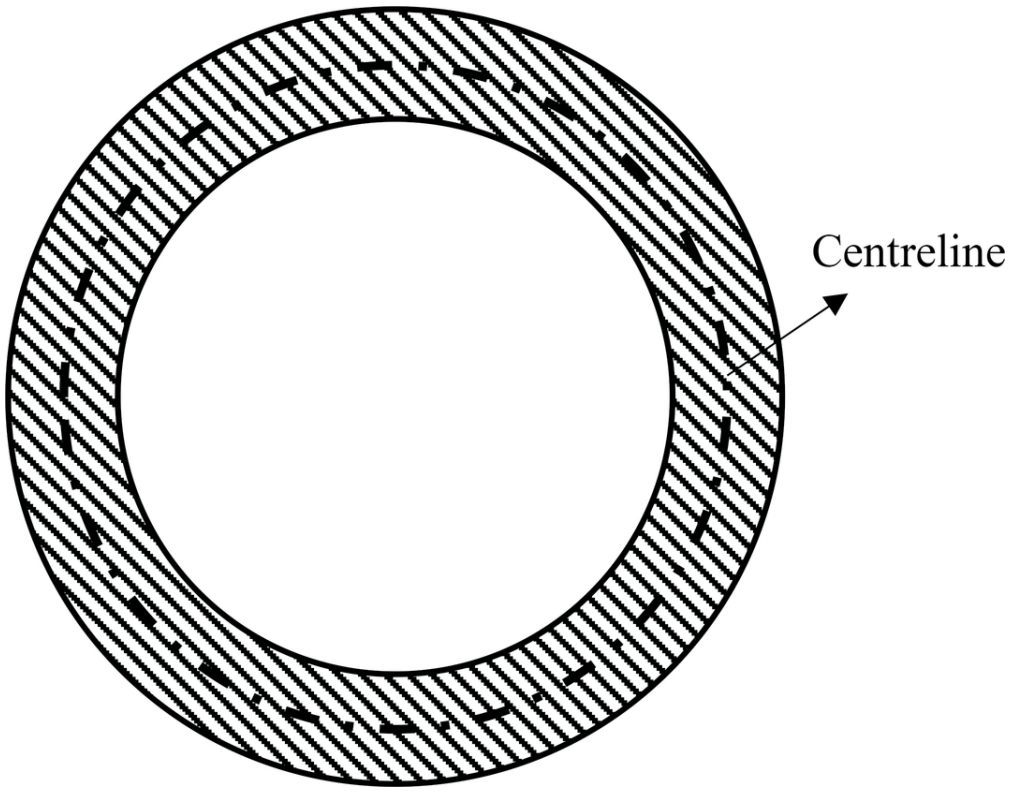

Fig. 9. Indication of the centreline of an annular cross-section of the flow channel.

90x70mm (300 x 300 DPI)

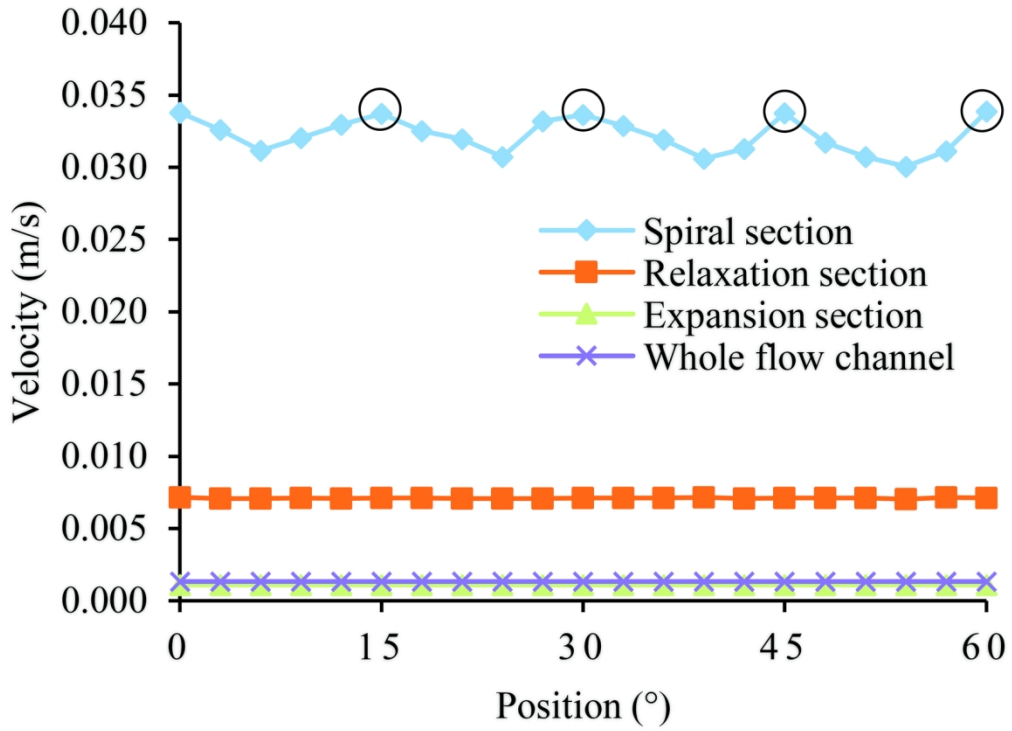

Fig. 10. Maximum velocity along the circumference at the annular exit of spiral section, relaxation section, expansion section and the whole flow channel.

73x53mm (600 x 600 DPI)

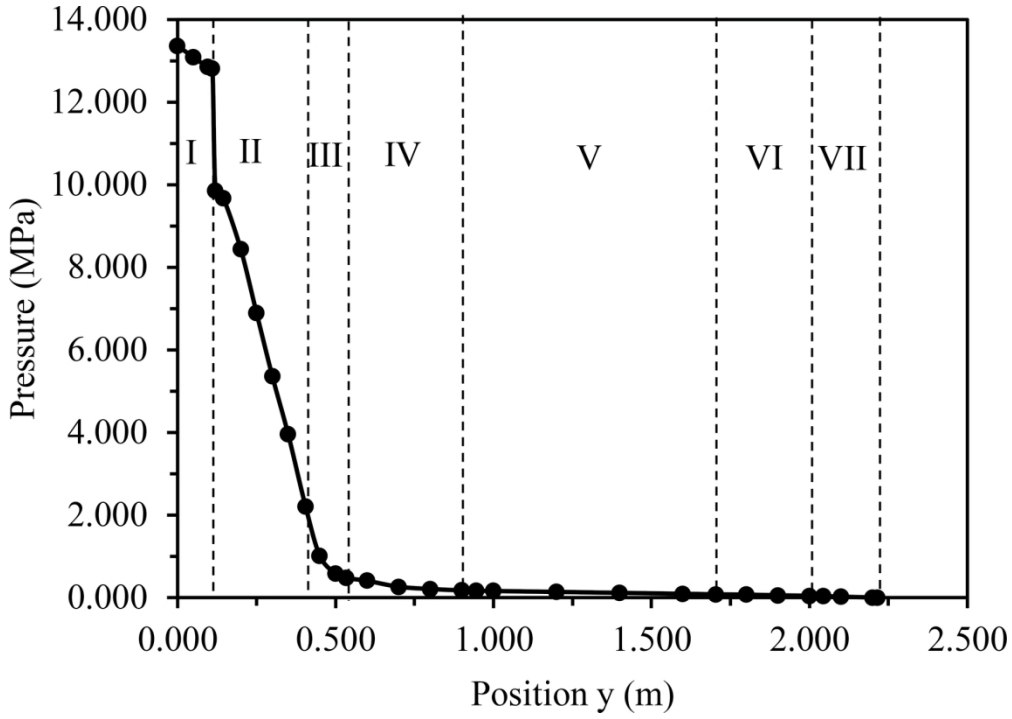

Fig. 11. Maximum pressure of cross-section at several positions along the axial direction (I: distribution section, II: spiral section, III: relaxation section, IV: expansion section, V: adapter section, VI: contraction section, VII: parallel section).

78x55mm (600 x 600 DPI)

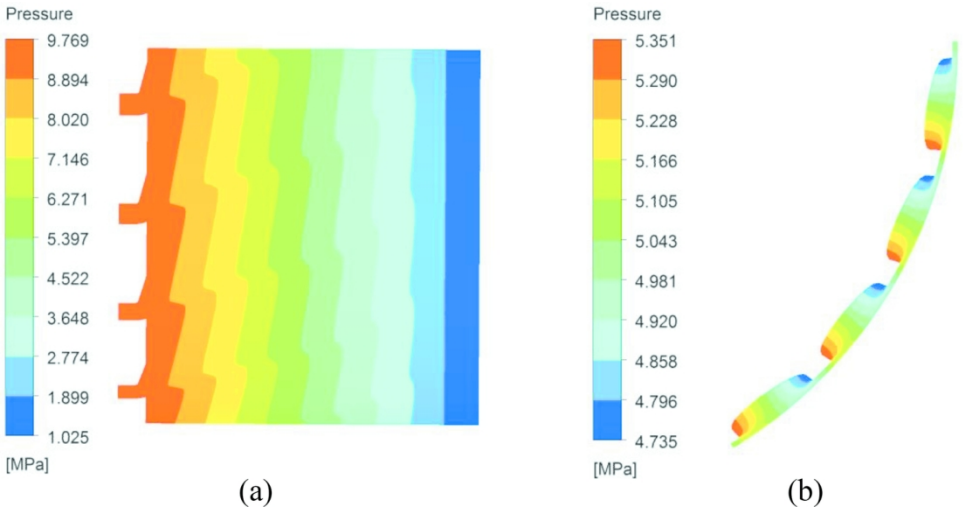

Fig. 12. Pressure distribution in spiral section (a: pressure distribution on the outer wall in spiral section, b: pressure distribution on the cross-section (y=0.3 m) vertical to axial direction in spiral section).

135x68mm (300 x 300 DPI)

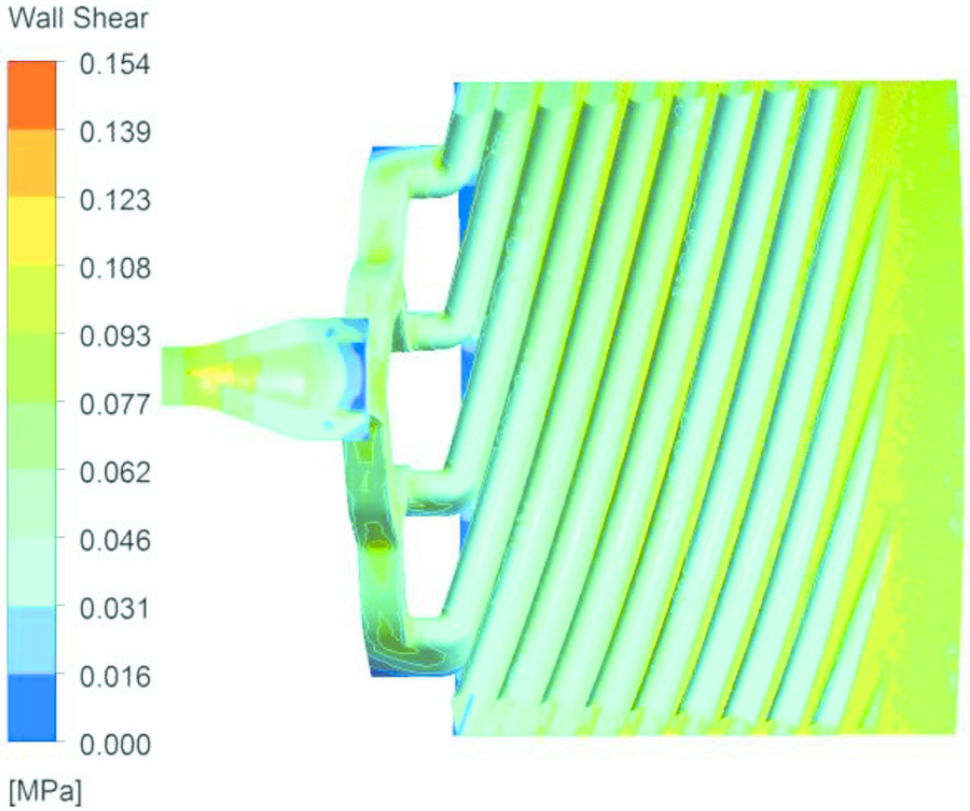

Fig. 13. Wall shear stress distribution in the distribution and spiral sections.

78x65mm (300 x 300 DPI)

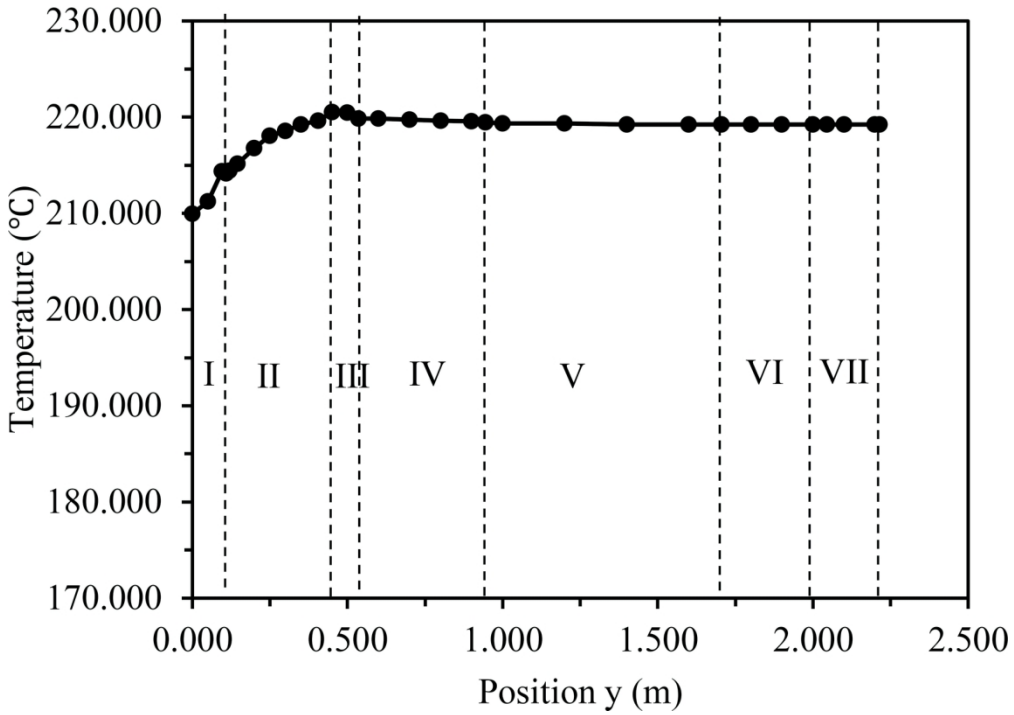

Fig. 14. Maximum temperature of cross-section at several positions along the axial direction (I: distribution section, II: spiral section, III: relaxation section, IV: expansion section, V: adapter section, VI: contraction section, VII: parallel section).

78x55mm (600 x 600 DPI)

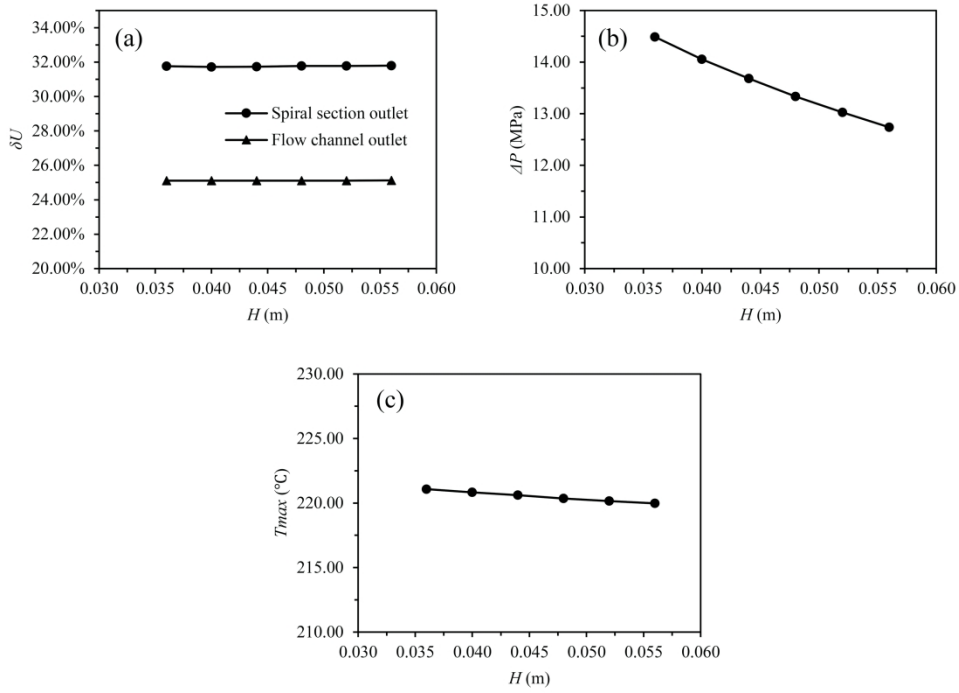

Fig. 15. Variations of (a) velocity relative deviation, (b) pressure drop and (c) maximum temperature versus different initial depths of spiral grooves.

139x101mm (600 x 600 DPI)

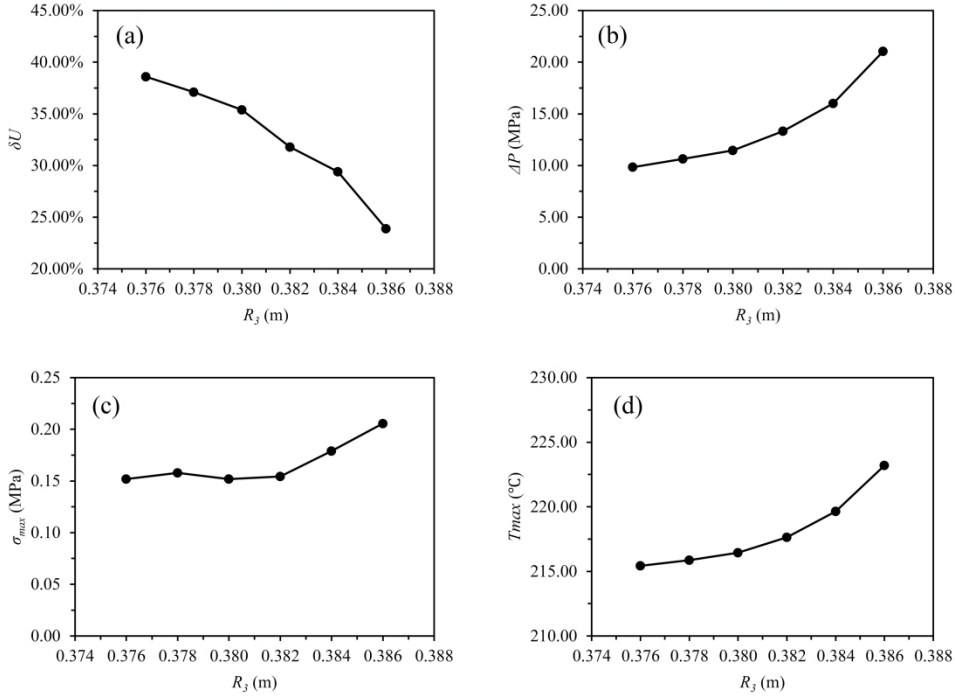

Fig. 16. Variations of (a) velocity relative deviation on the spiral section outlet, (b) pressure drop, (c) maximum wall shear stress and (d) maximum temperature versus different end radiuses of mandrel.

139x102mm (600 x 600 DPI)

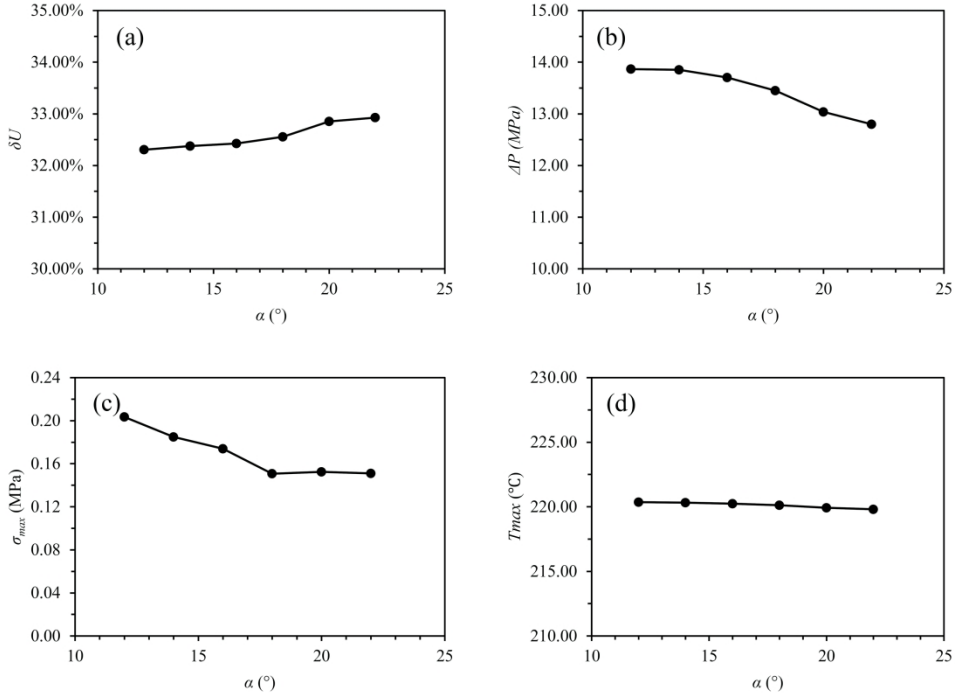

Fig. 17. Variations of (a) velocity relative deviation on spiral section outlet, (b) pressure drop, (c) maximum wall shear stress and (d) maximum temperature versus different helix angles.

139x102mm (600 x 600 DPI)

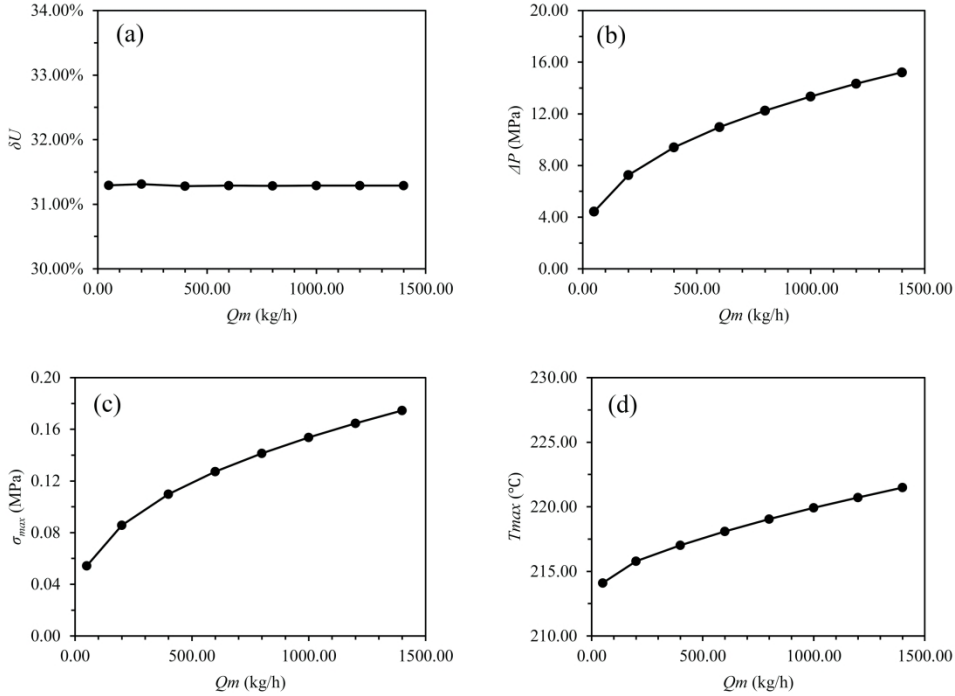

Fig. 18. Variations of (a) velocity relative deviations on spiral section outlet, (b) pressure drop, (c) maximum wall shear stress and (d) maximum temperature with different mass flow rates.

139x102mm (600 x 600 DPI)

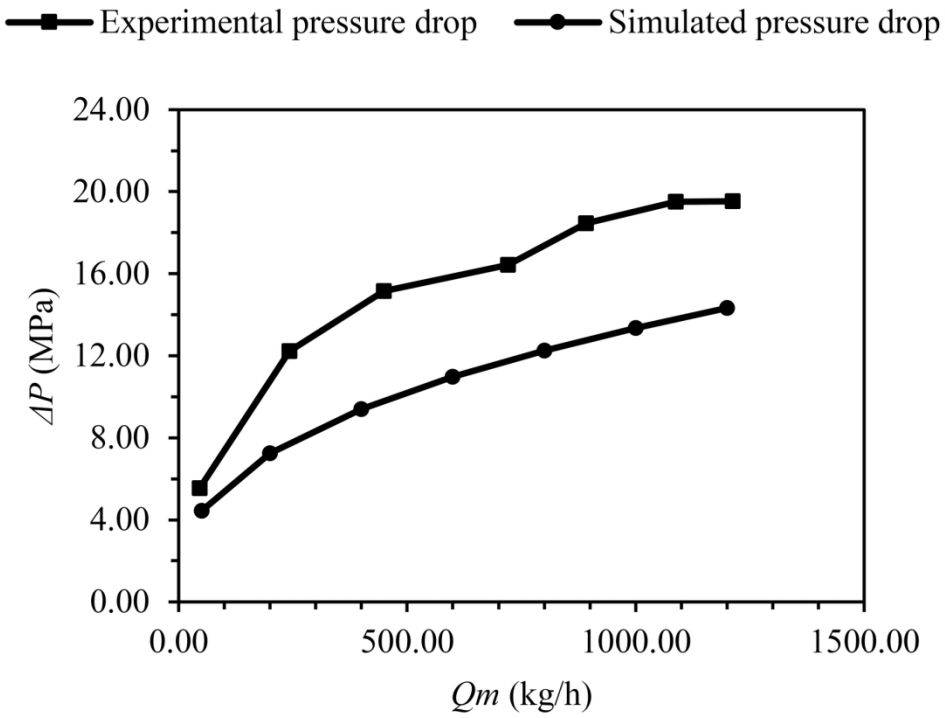

Fig. 19. Variation of experimental and simulated pressure drops versus different mass flow rate.

82x70mm (600 x 600 DPI)